Volume 1 | Number 1 | Jan 2013 | Pages 1–100

Nanoscale

www.rsc.org/nanoscale

ROYAL SOCIETY OF CHEMISTRY

This is an *Accepted Manuscript*, which has been through the Royal Society of Chemistry peer review process and has been accepted for publication.

Accepted Manuscripts are published online shortly after acceptance, before technical editing, formatting and proof reading. Using this free service, authors can make their results available to the community, in citable form, before we publish the edited article. We will replace this *Accepted Manuscript* with the edited and formatted *Advance Article* as soon as it is available.

You can find more information about *Accepted Manuscripts* in the **Information for Authors**.

Please note that technical editing may introduce minor changes to the text and/or graphics, which may alter content. The journal's standard **Terms & Conditions** and the **Ethical guidelines** still apply. In no event shall the Royal Society of Chemistry be held responsible for any errors or omissions in this *Accepted Manuscript* or any consequences arising from the use of any information it contains.

Journal Name

ROYAL SOCIETY
OF CHEMISTRY

ARTICLE

Nano-structured electron transporting materials for perovskite solar cells

Hefei Liu,[a] Ziru Huang,[a] Shiyuan Wei,[a] Lingling Zheng,[a] Lixin Xiao[abc]* and Qihuang Gong[a]*

Organic-inorganic hybrid perovskite solar cell has been developing rapidly in the past several years, whose power conversion efficiency has reached over 20%, getting close to that of polycrystalline silicon solar cell. Because the diffusion length of hole in perovskite is longer than that of electron, the performance of device can be improved by using an electron transporting layer, e.g., TiO_2, ZnO and TiO_2/Al_2O_3. Nano-structured electron transporting materials facilitate not only electron collection but also morphology control of perovskite. The property, morphology and preparation method of them are reviewed in the present. A comprehensive understanding of the relationship between the structure and property will benefit precise control of the electron transporting process and thus further improve the performance of perovskite solar cell.

1. Introduction

Organic-Inorganic hybrid perovskite solar cell (PSC) was investigated enthusiastically due to the excellent optical and electronic properties in the past two decades.[1-3] The organometal halide perovskite can be written as ABX_3, where X is a halogen ion (I^-, Br^-, Cl^-), A an organic ammonium ion, such as $CH_3NH_3^+$ (MA^+) and $NH=CHNH_3^+$ (FA^+), and B Pb^{2+} or Sn^{2+}. The most popular perovskite, $MAPbI_3$ and $MAPbI_{3-x}Cl_x$, both have a direct band gap of ~1.55 eV, corresponding to an absorption onset of 800 nm and intense absorption of the entire visible region.[4-6] In 2009, the perovskite was first used as a semiconductor sensitizer in liquid dye-sensitized solar cell (DSSC) with a power conversion efficiency (PCE) of 3.8%.[7] A solid-state mesoscopic solar cell based on $MAPbI_3$ was reported in 2012, whose PCE was enhanced to 9.7%.[8] Snaith et al. improved the PCE to 10.9% by using Al_2O_3 to replace the mesoporous TiO_2 as a pure scaffold.[9] Grätzel et al. fabricated a high-quality perovskite film by employing two-step sequential deposition method, and consequently obtained a high PCE of over 15%.[10] Yang et al. reported a planar PSC with a PCE of 19.3% using precise interface engineering.[11] Recently, the highest PCE has been reported as high as 20.1%,[12] getting close to that of polycrystalline silicon solar cell.[13]

Based on the unique property of perovskite, two typical architectures are usually constructed, i.e., mesoscopic structure and planar p-(i)-n junction structure. Figure 1 shows the schematic device structure and charge pathway. It was found that the diffusion length for hole was longer than that for electron in $MAPbI_3$.[14] To compensate the shorter electron diffusion length, an extra electron transporting layer (ETL) is used, so that electrons separated from photo-generated excitons can be injected to the ETL, then collected by fluorine-doped tin oxide (FTO) electrode.[15,16] In the case of mesoporous TiO_2, electrons can be transported not only through the perovskite but through the nanostructure scaffold, leading to better charge collection.[17] Besides, the ETL should also serve as a hole-blocking layer (HBL) in both two architectures to prevent hole from reaching the FTO electrode.

The design of ETL is crucial to determining the performance of PSC. Generally, to make highly efficient perovskite solar cell, series resistance (R_S) should be small while shunt resistance (R_{sh}) and recombination resistance (R_{rec}) should be large. The R_S normally reflects the resistance of photoactive layer and electrode, along with the contact resistance at each interface, which affects the short-circuit current density (J_{SC}) of device. Thus, the energy level of ETL is
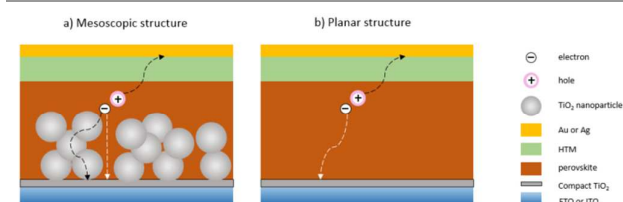
Fig. 1: Diagram of structure and electron transport mechanism of (a) mesoscopic structure and (b) planar structure. In mesoscopic structure, photo-generated electrons can be collected and transported by TiO_2 nanoparticles.

a. State Key Laboratory for Mesoscopic Physics and Department of Physics, Peking University, Beijing 100871, China. E-mail: lxxiao@pku.edu.cn; qhgong@pku.edu.cn
b. Beijing Engineering Research Center for Active Matrix Display, Beijing 100871, China
c. New Display Device and System Integration Collaborative Innovation Center of the West Coast of the Taiwan Strait, Fuzhou 350002, China

Nanoscale Accepted Manuscript

Hefei Liu is currently a research assistant at the Department of Physics, Peking University (China). He received his B.S. degree in physics from Peking University in 2015. His current research interest is on perovskite solar cells.

Lixin Xiao is a professor of the Department of Physics, Peking University (China) since 2011. He received his PhD in applied chemistry from The University of Tokyo (Japan) in 2000. He has been working on organic opto-electronics materials and devices, especially on photovoltaic (PV) and organic light-emitting-devices (OLED).

Qihuang Gong is an Academician of Chinese Academy of Sciences, Chengkong professor in Department of Physics at Peking University. He received his Bs and PhD in physics from Peking University, China, in 1983 and 1989, respectively. His research activities are focused on organic optoelectronics and photonics materials and devices.

supposed to be well-matched to that of perovskite to facilitate electron injection and hole blocking simultaneously, and the electron mobility of material is required to be high enough. In addition, the ETL should be porous to enhance the sufficient infiltration of the absorber. On the other hand, the R_{sh} tightly correlates with the leakage current due to the charge recombination or pinhole.[18] Then the HBL should be very thin and dense with few defects to obtain high open-circuit voltage (V_{OC}) and fill factor (FF). Recombination can also reduce photo-generated electron and result in lower J_{SC}, thus the recombination should be suppressed to give higher V_{OC} and J_{SC}.

Nanoscale semiconductors, including TiO_2, ZnO and insulators, such as Al_2O_3 and ZrO_2 are employed in PSC as ETL or scaffold. This review includes three parts according to the ETL material: TiO_2, ZnO and others. In each part, we systematically summarize the morphology control and modification of nanostructures. A comprehensive understanding of the relationship between the structure (geometry and morphology) and property could guide us to further optimize the design of ETL and to improve device performances. Moreover, the present study on low-temperature fabrication of ETL will help us to explore new practical methods for low-cost and high-performance PSC with mass production.

2. TiO_2

TiO_2 has been proved to be a leading electron transporting material (ETM) in PSC, with a conduction band minimum (CBM) of 4.1 eV[19] and a large band gap (3.2 eV for anatase phase[20] and 3.0 eV for rutile phase[21]). Its CBM is slightly lower than that of $CH_3NH_3PbI_3$, guaranteeing electron injection from perovskite absorber to ETL through direct contact, and its valence band maximum (VBM) is at a very low position, which gives TiO_2 an outstanding hole blocking property. Besides, the preparation and morphology control of TiO_2 has matured and been reported by most researchers. All these factors make TiO_2 a widely used material for ETL in PSC. There are two kind of TiO_2 morphologies applied in PSC: compact layer and mesoporous layer, whose properties such as energy levels, porosity, electron mobility, can be improved by various modifications, including different synthesis methods, doping, size/geometrical shape control and so on, was showed in Figure 2.

2.1 Compact layer

A thin compact TiO_2 film (10-100 nm) can be used as an excellent HBL, due to energy level alignment and high electron mobility (25 cm^2/Vs).[22] It's found that electron diffusion length of the compact layer is over 1 μm,[22] illustrating that thickness may not be the key factor. Actually, defects and crystal boundaries of compact TiO_2 act as electron traps, which would increase charge recombination, reduce V_{OC} and unstablize the device. In addition, there exist pinholes and cracks in the compact layer allowing the intimate contact between FTO electrode and perovskite or hole transporting layer (HTL), which further deteriorates the hole-blocking capability. Therefore, a thin uniform TiO_2 HBL with few defects and pinholes is important to achieve high efficiency.

Traditionally, as widely applied in DSSC, TiO_2 HBL is prepared by spin coating,[23] spray pyrolysis,[24-26] or sol-gel.[27] An ethanol (or 2-propanol) solution of titanium (IV) isopropoxide (~ 0.2 M), as a precursor, is spin coated or sprayed in short pulses onto a clean FTO glass substrate, then hydrolyzed and converted into TiO_2. In spray pyrolysis method, the substrate should be placed on a hotplate at about 500 °C. The thickness of the layer can be tuned by the concentration of the precursor, spin speed or the number of pulses. In sol-gel method, a dispersion of TiO_2 nanoparticles was obtained by adding titanium (IV) isopropoxide drop-wise into dilute nitric acid under constant stirring and heating. Only using solution and thermal treatment endues the three methods with easy operation and low cost. However, in many cases, pinholes, cracks and gaps between TiO_2 and FTO appear after the heat treatment (>450 °C) subsequent to the deposition, attributed to further

Nanoscale

crystallization and thermal stress, especially after sintering mesoporous TiO_2 scaffold. A comparison research shows that the HBL made by spin coating is highly porous, and the other by spray pyrolysis leads to good coverage and blocking action. Strikingly, the solar cells made with porous HBL reached slightly higher PCEs,[28] illustrating porous HBL can also prevent the contact between FTO and the HTL.

Although a compact perovskite layer can also reduce recombination, a high-quality TiO_2 HBL is still needed for better blocking property and reproducibility. Wu *et al.* fabricated TiO_2 compact layer with much lower density of nanoscale pinholes by atomic layer deposition (ALD).[29] TiO_2 was deposited in pulse mode at 200 ^{o}C using tetrakis (dimethylamino) titanium (TDMAT) and H_2O as Ti and O resources, respectively. ALD-TiO_2-based device exhibited high R_{sh} and at least 50% higher PCE compared with the device comprising TiO_2 layer fabricated by solution method. Magnetron sputtering (MS) is another general way to fabricate TiO_2 HBL. Ti film, coated on FTO glass by radio frequency magnetron sputtering from Ti target, is oxidized and converted to a thin TiO_2 compact film during sintering process.[30] PSC with TiO_2 compact film prepared by thermal oxidation has lower dark current density, lower R_S and higher R_{rec} than those of two-step sintering, resulting in higher J_{SC} and FF. But the thermal oxidation process might leave residue of Ti nanoparticles, consequently increasing the recombination of charge. TiO_2 compact film can also be prepared by directly sputtering TiO_2 target onto FTO glass, leading to a direct and full-range contact between MS-TiO_2 and FTO, which contributes to fast and effective transportation of electrons,

leading to high J_{SC}.[31] Morphology of TiO_2 compact layers fabricated by different methods is showed in Figure 3.

Another way to improve the properties of TiO_2 compact film is doping. Wang *et al.* added magnesium acetate tetrahydrate into $TiCl_4$ solution and obtained Mg-doped TiO_2 compact film.[32] Mg in the blocking layer elevated the position of the CBM of TiO_2, contributing to the improvement of V_{OC}. Besides, there was also a thin layer of magnesium oxide and magnesium hydroxide formed at the surface of HBL, which could suppress the charge recombination at the compact TiO_2 surface, achieving a further improvement of V_{OC}. A low level of Al-doping by adding aluminium isopropoxide precursor to Ti (IV) isopropoxide solution, can reduce non-stoichiometric oxygen-induced defects in TiO_2,[33,34] attributed to the substitution of two Al (III) for two adjacent Ti (III) with an oxygen vacancy. The substitution removes deep electronic traps and sub-bandgap states, enhances the conductivity by orders of magnitude, and improves the stability of devices.[35] A Nb-doped TiO_2 compact layer was prepared via spray pyrolysis. Thus both the blocking effect and forward electron transport were improved. It was found that Nb-doping decreased R_S of the device, resulting in higher J_{SC} and FF.[36] A high-efficiency device has been realized by employing yttrium-doped TiO_2 compact layer.[11] The existence of yttrium brings about a higher conductivity of TiO_2, possibly attributed to higher carrier concentration, which matches that of 2,2',7,7'-tetrakis(N,N-di-p-methoxyphenylamine)-9,9-spirobifluorene (spiro-OMeTAD), and enhances J_{SC} and FF. Wang *et al.*[37] reported graphene nanoflakes modified TiO_2 HBL by spin coating a dispersion of graphene-TiO_2 nanocomposites. The graphene flakes were fully
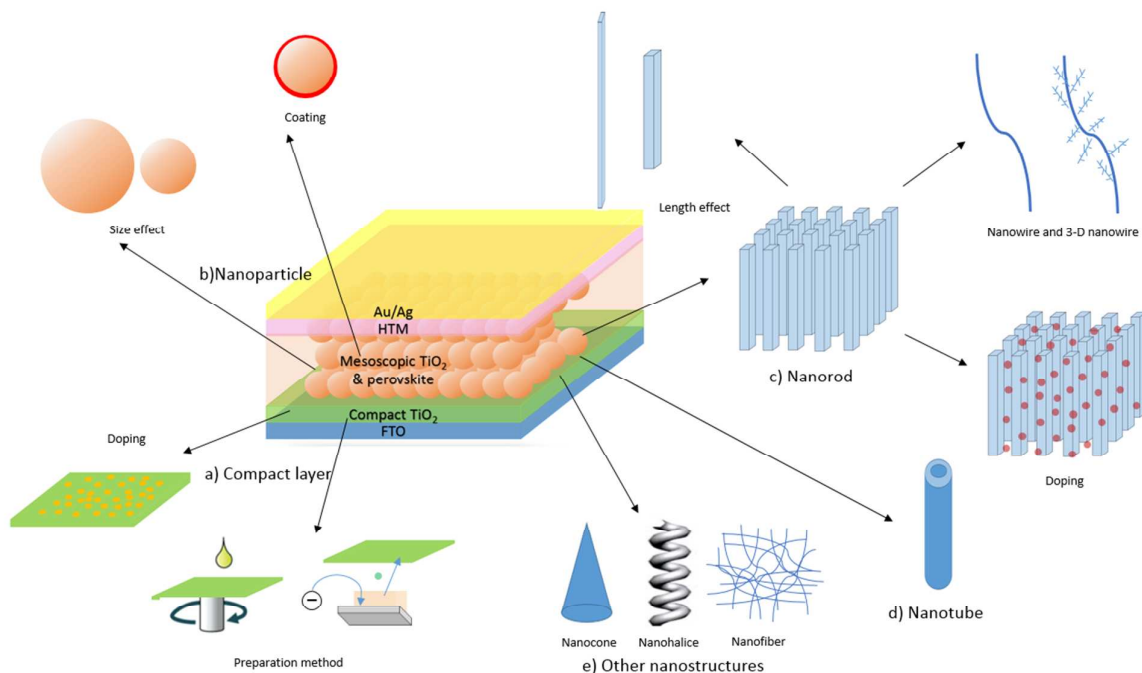
Fig. 2: Schematic illustration of various nanostructures and modifications of TiO_2 in PSC.

Table 1 Summary of PSCs with modifications in compact TiO_2 layer

Fabrication method of compact TiO_2 layer	Device structure	J_{SC} (mA/cm^2)	V_{OC} (V)	FF	PCE(%)	Ref
Spin coating	FTO/bl-TiO_2/mp-TiO_2-MAPbI$_3$/spiro-OMeTAD/Au	20.80	0.95	0.74	14.6	28
Spray pyrolysis	FTO/bl-TiO_2/mp-TiO_2-MAPbI$_3$/spiro-OMeTAD/Au	20.70	0.95	0.72	14.2	28
Atomic layer deposition	FTO/bl-TiO_2/mp-TiO_2-MAPbI$_3$/spiro-OMeTAD/Au	18.74	0.93	0.72	12.6	29
Thermal oxidation	FTO/bl-TiO_2 /mp-TiO_2-MAPbI$_3$/spiro-OMeTAD/Au	21.97	1.09	0.63	15.1	30
Magnetron sputtering	FTO/bl-TiO_2/MAPbI$_3$/P3HT/Ag	20.99	1.00	0.49	10.2	31
Spin coating	FTO/bl -Mg-TiO_2/mp-TiO_2-MAPbI$_3$/spiro-OMeTAD/Au	18.34	1.08	0.62	12.3	32
Spray pyrolysis	FTO/bl-Nb-TiO_2/mp-TiO_2-MAPbI$_3$/spiro-OMeTAD/Au	18.08	0.88	0.65	10.3	36
Sol-gel	ITO/PEIE/ bl-Y-TiO_2/MAPbI$_{3-x}$Cl$_x$/ spiro-OMeTAD Au	22.75	1.13	0.75	19.3	11
Spin coating	FTO/graphene-TiO_2/mp-Al$_2$O$_3$-MAPbI$_3$/spiro-OMeTAD/Au	21.90	1.04	0.73	15.6	37

*bl-: blocking layer, mp-: mesoscopic porous

coated by TiO_2 nanoparticles, acting as electron collectors, thus increasing R_{rec}. The high charge mobility of grapheme reduces R_S, and consequently enhances FF and PCE. These works demonstrate that graphene or metal oxide doping has the potential to improve charge transport. Table 1 shows the performance of devices with these modifications in compact layer.

Except blocking capability, obtaining TiO_2 compact layers with lower cost is important as well. High temperature treatment, the most energy consuming process, obstructs the road towards roll-to-roll processing on flexible foils that can withstand no more than 150 ^{o}C. Thus, low-temperature fabricating methods are proposed. The graphene-TiO_2 nanocomposites based device,[37] using graphene as electron collector and an Al$_2$O$_3$ scaffold, can be fabricated at a temperature less than 150 ^{o}C. Yella et al.[38] employed a chemical bath deposition process. By immersing FTO into diluted TiCl$_4$ solution and heating at 70 ^{o}C, electrodes with a thin layer of crystalline TiO_2 (rutile) nanoparticles were prepared. Snaith et al.[39] fabricated a low temperature TiO_2 compact layer by spin coating a colloidal dispersion of anatase particles synthesized by sol-gel method[40] in anhydrous ethanol, formulated with titanium diisopropoxide bis(acetylacetonate) (TiAcAc), followed by drying at 150 ^{o}C. TiAcAc serves as "electronic glue" between the nanoparticles in thin film, enhancing its conductivity and thus improving PCE. The above-mentioned two methods both use TiCl$_4$, which would produce HCl fume when in contact with humidity. Another low-temperature method using titanium isopropoxide as titanium source was reported.[41] The layer is deposited from TiO_2 nanoparticle dispersion with TiAcAc and annealed at 135 ^{o}C in air. A planar heterojunction perovskite solar cell with high PCE of 13.6% makes this method promising in large scale manufacture.

2.2 Mesoporous layer

2.2.1 Nanoparticle

The meso-structured device generally employed a layer of mesoporous TiO_2 or Al$_2$O$_3$ (several-hundred-nanometer thick) as the scaffold, so as to facilitate the crystallization of the perovskite with enhanced nucleation at the nanoparticles'

surface,[42] and enlarge the contact area between perovskite and the ETL to efficiently collect photo-generated electrons. It's found that photo-electrons are injected to TiO_2 nanoparticles then transported to compact layer and FTO for devices with TiO_2 scaffold;[9,43] by contrast, the dominant electron transport pathway is the perovskite absorber in devices with Al$_2$O$_3$ scaffold due to its high CBM.[9] Thus TiO_2 scaffold is also called electron collecting layer. Usually, a sintering process is subsequent to the deposition of TiO_2 scaffold to enhance electronic connectivity. Further research showed that even though TiO_2 nanoparticles share the same transport rate with compact TiO_2, the recombination rate is higher for mesoscopic
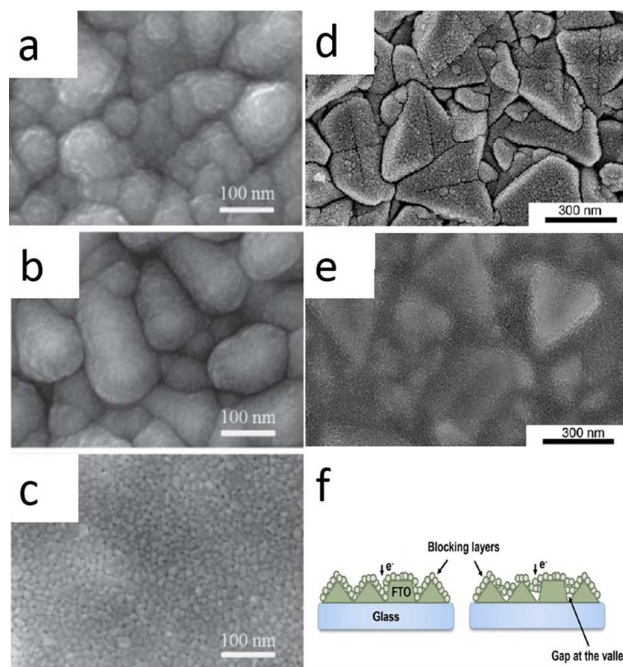
Fig. 3: Top-view FE-SEM images of TiO_2 compact layers fabricated on FTO electrodes by different preparation methods: (a) Atomic layer deposition, (b) spray pyrolysis, (c) spin coating, (d) magnetron sputtering and (e) sol-gel, and (f) an illumination diagram of these images. (a), (b) and (c) reproduced from ref. 29 with permission from the Japan Society of Applied Physics. (d), (e) and (f) reproduced from ref. 31 with the permission from the Chemical Society of Japan.

structure, ascribed to shorter electron diffusion length.[44] Permeability and electron transport should be simultaneously concerned in designing mesoporous TiO_2 layers. Mesoporous TiO_2 scaffold is usually prepared by screen-printing or spin coating a commercial paste composed of TiO_2 particles (like 18NR-T), or by evaporating a weakly alkaline solution containing Ti^{4+} and H_2O_2.[45-47] TiO_2 nanoparticles can also be synthesized by sol-gel method.[39-41,48,49] The size of particles can be very small (~15 nm) and easily controlled by the concentration, pH and heating temperature.

The size of the TiO_2 nanoparticles is crucial to determining the properties of scaffold, despite there are few reports about it in PSC. Generally, if the size is too small, the pore will be dense and small, resulting in close pores forbidding infiltration of perovskite. On the other hand, excessively large particles will add further complication for controlling the morphology of perovskite, increasing the risk of intimate contact between TiO_2 nanoparticles and HTL. In addition, the total pore volume decreases as the increase of particle size,[49] which is destructive to the light absorption of perovskite that subsequently fills the pores. Thus, controlling the size of TiO_2 nanoparticles into a proper scale is essential to high efficiency. Han *et al.* investigated size effect of TiO_2 nanoparticles in a hole-conductor-free mesoscopic perovskite solar cell with ZrO_2 layer and carbon electrode.[49] The results indicate that the size of TiO_2 particles affects not only the infiltration and contact of the perovskite, but also the charge transfer kinetics at the perovskite/TiO_2 interface. Both R_S and R_{rec} decrease with the increase in size of TiO_2 nanoparticles, possibly attributed to the electronic contact between TiO_2 and carbon electrode. The device with particles of 25 nm diameter exhibits the best PCE of 13.4%. Seok *et al.*[50] reported well-organized mesoporous TiO_2 layer with enlarged pores through a copolymer-induced sol-gel assembly method. The cell fabricated with 15 nm (pore diameter) mesoporous layer is superior to that of 10 nm layer, demonstrating the importance of the size effect in meso-structure solar cells.[49,50]

A single-crystal TiO_2 mesoporous layer that provides both desired highly accessible surfaces and good electronic connectivity is reported in DSSC.[51] However, to our best knowledge, this technique has not been applied in PSC. Instead, researchers usually fabricate an extra thin hole blocking layer on the surface of mesoporous layer to suppress recombination of carriers. Sub-nanometer conformal TiO_2 overlayers (1-4 nm thick) were deposited by ALD, which led to an overall reduction in the passivation layer capacitance, discouraging electron recombination and resulting in a higher V_{OC}, PCE was improved by over 50% with the addition of overlayer.[52] The overlayer bring about better connection between nanoparticles, which makes sintering unnecessary and consequently, the whole fabrication can be processed at low temperature. Park *et al.*[53] covered the TiO_2 mesoporous layer with MgO by spin coating. The magnesium methoxide solution was drop wise added onto the mesoporous layer. Magnesium methoxide molecules would be chemisorbed onto the surface of TiO_2 by reacting with surface hydroxyl groups and the absorbed water, which leads to the formation of MgO ultrathin layer to retard

charge recombination, thereby extending the carrier life-time. Devices employing MgO-coated TiO_2 films exhibited an increase in FF and V_{OC} but a decrease in photocurrent because of the insulating nature of MgO, so that PCE is enhanced only a little. Qin *et al.*[54] employed yttrium to modify the electronic structure of TiO_2 by an aliovalent substitution of cations in crystal lattice. Yttrium's poor solubility in TiO_2 makes Y_2O_3 only appear on the surface of TiO_2. Thus, adding YCl_3 to titanium isopropoxide solution in the synthesis of nanoparticles is an alternative way. Yttrium's ability to block electron recombination results in 15% increase of J_{SC}.

Another way to improve transport properties of mesoporous TiO_2 layer is to add electron acceptors, such as C_{60} and graphene.[55,56] C_{60}-coated TiO_2 nanoparticles are obtained by immersing the substrates in C_{60}-substituted benzoic acid self-assembled monolayer ($C_{60}SAM$) solution. The $C_{60}SAM$ acts as an electron acceptor to decline in electron back reaction but inhibit further electron transfer into TiO_2 nanoparticles due to energy level misalignment and poor electronic coupling, thus thermalized electrons from $C_{60}SAM$ are then transported to perovskite phase. Though $C_{60}SAM$ can only reduce V_{OC} loss, the device still achieved a PCE as high as 11.7%.[55] By electrochemical method,[57] a thin layer of graphene quantum dots (GQDs) was deposited between perovskite and TiO_2. The induced photon-to-current conversation efficiency (IPCE) and absorbed photon-to-current conversation efficiency (APCE) spectra show electrons can be extracted from photo-generated excitons faster (90-106 ps) with GQDs than without it (260-307 ps), which boosts the photocurrent, consequently improving J_{SC} and FF.[57]

2.2.2 Nanorod and nanowire

Highly crystalline TiO_2 nanorod has been applied in PSC for its advantages, such as open porous structure, easily controllable diameter and length, and two orders of magnitude higher electron mobility than particulate TiO_2.[58] TiO_2 nanorods can be synthesized through a variety of methods such as metal organic chemical vapour deposition (MOCVD),[59] electrochemical anodization[60] and hydrothermal method.[58,61] In particular, hydrothermal synthesis is a low-temperature, facile approach without requirement of expensive facilities, so that it is widely adopted and suitable for large-scale application. In a typical hydrothermal synthesis,[61] Ti precursors are added into water or organic solutions under strong acidic condition. Because strong acids will increase the equipment cost and cause environmental damage, recently an acid-free medium growth method employing disodium ethylenediamine tetraacetate (Na_2EDTA) is reported, and PSC with the as-made rutile TiO_2 shows a PCE up to 11.1%.[62]

A research about length effect in TiO_2 nanorods shows that charge recombination rate is similar in nanorods with different length but electron diffusion is faster in longer nanorod. Strikingly, V_{OC}, J_{SC} and PCE degrade with increase of nanorod length, which is illustrated as the disorder in longer nanorods array, aggravating the pore filling.[58] On the other hand, for significant mesoscopic effect, TiO_2 nanorods shouldn't be too short, or the device will be more similar to planar-structure

PCSs. A comparison research[63] shows that though a planar architecture provides higher initial V_{OC} and PCE, a TiO_2 nanorods layer is crucial to achieving long term durable performance of PSC. So the length of TiO_2 nanorods is supposed to be well-designed.

The morphology of TiO_2 nanorods can be tuned by various modifications. Similar to TiO_2 nanoparticles,[52] an ultrathin TiO_2 block layer was deposited on the surface of TiO_2 nanorods by ALD, which facilitates a low recombination rate with a high V_{OC}, leading to a good FF and PCE.[64] Metal ion doping can improve the performance of TiO_2 nanorods layer as well, e.g., Mg doping[65] can elevate the CBM of TiO_2, suppressing recombination but increasing R_S; Nb and Sn doping result in lower R_S and higher R_{rec} by facilitating electron transport through perovskite/TiO_2 interface.[66,67] The PCEs of devices based on these doped TiO_2 nanorods are higher than those of devices with undoped TiO_2 in each research by about 33%, 50% and 67% for Mg, Nb and Sn, respectively.

Nanorods would evolve to bendable nanowires as the increase of ratio between length and diameter under controllable conditions.[68] A thinner diameter facilitates the infiltration of perovskite,[69] allowing a thicker mesoporous TiO_2 layer to load more perovskite for higher absorption, resulting in improved PCE.[70] By fabricating rugged surface through ALD, TiO_2 nanowires can be further modified to become 3D nanowires, exhibiting advantages in terms of electron delivering and light scattering.[71]

2.2.3 Nanotube

Unlike nanoparticle or nanowire, TiO_2 nanotube arrays can be employed as perovskite hosts to improve infiltration and light absorption. Besides, a reduced charge recombination in nanotube electrodes is observed, contributing to higher PCE. Yuan *et al.*[72] obtained a freestanding TiO_2 nanotube array prepared by two-step electrochemical anodization and achieved 6.5% of PCE with 2.3 μm of TiO_2 nanotubes. However, restricted by synthesis method, TiO_2 nanotube arrays are too thick (over 2 μm). This means electrons have to travel longer to be collected by electrodes, which exacerbates charge extraction and accumulation efficiency, hindering J_{SC} and PCE. Wong *et al.*[73] fabricated aligned TiO_2 nanotube arrays on Ti foil using electrochemical anodization and employed carbon nanotube (C_{120}) as transparent counter electrode. 8.3% of PCE was obtained with 300 nm in length and 60 nm in diameter of tubes. Such devices with double nanotube layer are highly flexible, maintaining good performance after 100 bending cycles.

2.2.4 Other nanostructures

Other nanostructures of TiO_2 were prepared by manipulating the growth process. TiO_2 nanofiber was electrospun directly on TiO_2 compact layer with $TiCl_4$ treated rough surface.[74] However, device using this structure exhibited unsatisfying efficiency because of poor conversion from PbI_2 to $CH_3NH_3PbI_3$ in nanofiber layer. Nanocones are obtained by fusing the nanorods consisting of ultrathin nanowires along the growth direction by adding Na_2EDTA into medium of hydrothermal process. Nanocone provides faster electron

transfer than nanorod, thus beneficial to suppressing charge recombination and improving the performance of devices.[75] Nanohalices are obtained by an oblique-angle deposition technique using an electron-beam evaporator on a silicon wafers. Nanohelical TiO_2 plays an important role in the suppression of hysteresis, since capacitive charges are likely to be quickly dissipated by charge separation in the presence of nanohalices. So no difference in current density-voltage curves in forward and reverse scanning modes were observed.[76] The morphology of mosoporous layers with these nanostructures is showed in Figure 4. Furthermore, with oblique-angle deposition, by adjusting the deposition conditions, such as tilt angle, substrate rotation speed, time interval between substrate rotation, and deposition rate, a variety of 3D nanostructures, including different nanohalices, slanted nanorods, and nano zig-zags, were produced with precise control of geometrical shape.[77-79] PSCs with these TiO_2 nanostructures are summarized
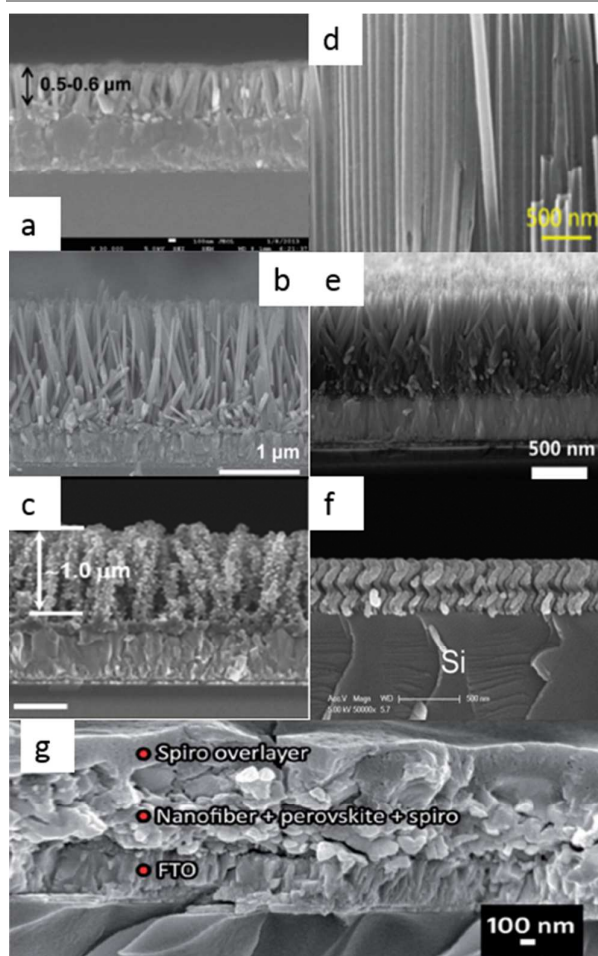
Fig. 4: Cross-section FE-SEM images of TiO_2 (a) nanorod, (b) 1-D nanowire, (c) 3D nanowire, (d) nanotube, (e) nanocone, (f) nanohalice and (g) nanofiber. (a) reproduced from ref. 58 with permission from the American Chemical Society. (b) reproduced from ref. 69 with permission from The Royal Society of Chemistry. (c) reproduced from ref. 71 with permission from the American Chemical Society. (d) reproduced from ref. 72 with permission from The Royal Society of Chemistry. (e) reproduced from ref. 75 with permission from Elsevier Ltd. (f) reproduced from ref. 76 with permission from The Royal Society of Chemistry. (g) reproduced from ref. 74 with permission from The Royal Society of Chemistry.

in Table 2. Because of its sufficient maneuverability of preparation process, more and more TiO_2 nanostructures are expected to be applied in PSC.

3. ZnO

ZnO is another important II-VI semiconductor with 4.2 eV of CBM, 3.3 eV of direct band gap and 60 meV of exciton binding energy at room temperature.[80,81] Since the LUMO and HOMO of perovskite $CH_3NH_3PbI_3$ are 3.6 eV and 5.2 eV, respectively,[82] efficient electron extraction and dissociation of excitons are expected.

Compared to TiO_2, ZnO has advantages, e.g., the conductivity of ZnO is several orders of magnitude higher than that of TiO_2,[83,84] so recombination loss will be less due to higher electron mobility.[85] Besides, high temperature sintering process is not necessary for the fabrication of ZnO,[86-88] which means that it can be used in flexible solar cells.[89] Its wurtzite structure has strong polarity in the c-axis direction, so the crystallization and anisotropic growth is superior, results in complex nanostructures and morphologies. Moreover, ZnO has excellent optical properties such as high infrared reflectivity and transparency in the visible spectrum. In addition, it is abundant in nature and inexpensive.[85] These interesting properties make it a promising ETL in PSCs. However, like TiO_2, ZnO also suffers from photocorrosion, which will reduce the performance and stability.[90,91]

The two main kinds of nanostructures in TiO_2: compact films and mesoporous structure with nanorods, are also applied in ZnO. Usually, films formed by nanoparticles have slower electron transport due to grain boundaries, which also cause higher recombination. Nanorods, however, have an internal electrical field in the direction of c-axis to enhance charge transport and refrain the recombination of injected electrons.[92]

3.1 Compact layer

To date, many perovskite solar cells with ZnO as the ETL consist of a compact ZnO layer, which functions as a hole blocking layer, preventing charge recombination. Without the ZnO layer, FF and V_{OC} are very low because of increased recombination at the ITO surface and a correspondingly low R_{sh}.[93] Zhang et al. used electrochemical deposition to generate a ZnO layer made of large grains with an average size of 300 nm.[94] The FF of the best-performing device is only 0.50, and it increases with the roughness of the ZnO-perovskite interface. Since the conductivity of ZnO layer is rather high, the low FF may be attributed to the charge transfer resistance at the interfaces. Hu et al. used ALD to fabricate a compact ZnO layer at 70 °C, and then deposited a 350 nm thick mesoporous Al_2O_3 layer.[86] After that, they used a single-step method to construct perovskite solar cell. A PCE of 13.1% was achieved, and the effective area was defined as 0.04 cm^2.[81] The ZnO layer is more condense than that of solution-processed ZnO layers so that it can more effectively suppress charge recombination. Adding other dopants can improve the energy level alignment, tune the surface morphology and suppress recombination.

Mahmood et al. used electrospraying and spin-coating to obtain ZnO and Al-doped ZnO films.[95] The morphology of the films can be easily controlled by changing deposition conditions. The V_{OC} of Al-doped ZnO based perovskite solar cell was improved due to higher electron concentration in the conduction band of ETL and lower recombination rate. Organic compounds can also improve the performance of PSC with ZnO compact layer. For example, as discussed in our previous review, [6,6]-phenyl C_{61} butyric acid methyl ester (PCBM), a widely used electron acceptor in perovskite solar cells,[96] can tune the energy level of ZnO. Kim et al. deposited 30 nm-thick sol-gel processed ZnO onto ITO and spin-coated PCBM onto the ZnO film.[82] The CBM of ZnO/PCBM is located between that of ZnO and that of perovskite, facilitating cascade charge extraction and higher V_{OC}. The R_{rec} of the device with ZnO/PCBM is higher, which means that adding PCBM can suppress surface charge recombination as well as bulk charge recombination.[97] However, solar cells with only PCBM on ITO exhibited poor performance. So they concluded that the synergic effect of ZnO and PCBM is essential for high performance.[82] Zhang et al. deposited 3-aminopropanoic acid SAM (C3-SAM) onto the sol-gel ZnO.[81] It was found that C3-SAM made perovskite crystals in more plate-like shape, enhancing light absorption. The PCE was improved from 11.2% to 15.7%.

Compact layers can be formed by spin coating a dispersion of ZnO nanoparticles without sintering, which is convenient to flexible cells. Song et al. spin-coated ZnO nanoparticles ETL and achieved 13.9% of PCE.[92] PCE degraded negligibly over 20 days, while it decreased to 20% of the initial value without the ZnO layer. The authors attribute the stability of the ZnO-based PSC to a nicely controlled PbI_2 passivation. Zhou et al. spin-coated ZnO nanoparticles on FTO and flexible ITO/Polyethylene Naphthalate (PEN) substrate.[87] They got PCE of 8.7% for the FTO device and 4.3% for the flexible device. The flexible devices maintain 80% of their initial PCE after 1000 times of bending. Liu et al. produces ZnO crystalline nanoparticles with 5 nm in diameter, then spin-coated on ITO/glass and ITO/poly(ethylene terephthalate) (PET) substrate to form compact ZnO layers.[88] Perovskite crystallites larger than 75 nm are observed on the interface between ZnO and perovskite. Large crystallites also act as scattering centres for incoming light, increasing effective optical path length of the device. The PCE of devices based on ITO/glass is 15.7%, and the PCE of flexible devices is 10.2%. Bending tests show that the flexible devices also perform well.

3.2 Mesoporous layer with nanorods

Another widely used structure is ZnO nanorods. Liang et al.[89] used magnetron sputtering to obtain ZnO films consisting of aligned ZnO nanorods. The J_{SC} is found to be larger than devices with ZnO nanoparticles and devices with compact or mesoporous TiO_2. It was found that after the deposition of 40 nm thick ZnO, the sheet resistance of ITO decreased more than 25%. This can be explained by the good conductibility of the c-axis oriented ZnO nanorods. Kumar et al. compared performances between devices with ZnO nanoparticles and

Table 2 Summary of PSCs with modifications in mesoporous TiO$_2$ layer

Morphology of mesoporous TiO$_2$	Device structure	J_{SC} (mA/cm^2)	V_{OC} (V)	FF	PCE(%)	Ref
Nanoparticle	FTO/bl-TiO$_2$/mp-TiO$_2$-(5-AVA)$_x$(MA)$_{1-x}$PbI$_3$/ZrO$_2$/C	22.9	0.87	0.67	13.4	49
Nanoparticle	FTO/bl-TiO$_2$/mp-TiO$_2$-MAPbI$_{2.7}$Br$_{0.3}$/PTAA/Au	18.8	1.04	0.66	12.8	50
Nanoparticle	FTO/mp-TiO$_2$- ALD-TiO$_2$-MAPbI$_3$/spiro-OMeTAD/Au	17.6	0.97	0.67	11.5	52
Nanoparticle	FTO/bl-TiO$_2$/ Mg-mp-TiO$_2$-MAPbI$_3$/ spiro-OMeTAD/Ag	20.0	0.89	0.71	12.7	53
Nanoparticle	FTO/bl-TiO$_2$/Y$_2$O$_3$-mp-TiO$_2$-MAPbI$_3$/ spiro-OMeTAD/Au	18.1	0.94	/	11.2	54
Nanoparticle	FTO/bl-TiO$_2$/C$_{60}$SAM-mp-TiO$_2$-MAPbI$_{3-x}$Cl$_x$ / spiro-OMeTAD/Ag	19.6	0.84	0.72	11.7	55
Nanoparticle	FTO/bl-TiO$_2$/graphene-mp-TiO$_2$-MAPbI$_3$/ spiro-OMeTAD/Au	17.1	0.94	0.64	10.2	57
Nanorod	FTO/bl-TiO$_2$/mp-TiO$_2$-MAPbI$_3$/ spiro-OMeTAD/Au	18.6	0.97	0.62	11.1	62
Nanorod	FTO/bl-TiO$_2$/mp-TiO$_2$- ALD-TiO$_2$- MAPbI$_3$/spiro-OMeTAD/Au	19.2	0.93	0.70	12.5	64
Nanorod	FTO/bl-TiO$_2$/ Mg-mp-TiO$_2$-MAPbI$_3$/Li-doped P3HT/Au	10.4	0.80	0.50	4.2	65
Nanorod	FTO/bl-TiO$_2$/ Nb-mp-TiO$_2$-MAPbI$_{3-x}$Br$_x$/ spiro-OMeTAD/Au	16.5	0.87	0.52	7.5	66
Nanorod	FTO/bl-TiO$_2$/ Sn-mp-TiO$_2$-MAPbI$_3$/ spiro-OMeTAD/Au	14.9	0.74	0.52	6.3	67
1D Nanowire	FTO/bl-TiO$_2$/ mp-TiO$_2$-MAPbI$_3$/ spiro-OMeTAD/Au	22.3	0.77	0.68	11.7	70
3D Nanowire	FTO/bl-TiO$_2$/ mp-TiO$_2$-MAPbI$_3$/ spiro-OMeTAD/Ag	14.8	0.95	0.64	9.0	71
Nanotube	Ti foil/ bl-TiO$_2$/ mp-TiO$_2$-MAPbI$_3$/ C$_{120}$ + spiro-OMeTAD	12.6	0.97	0.60	7.4	73
Nanofiber	FTO/bl-TiO$_2$/ mp-TiO$_2$-MAPbI$_3$/ spiro-OMeTAD/Au	15.9	0.98	0.63	9.8	74
Nanocone	FTO/bl-TiO$_2$/ mp-TiO$_2$-MAPbI$_3$/ spiro-OMeTAD/Au	19.5	0.92	0.62	11.0	75
Nanohalice	FTO/bl-TiO$_2$/ mp-TiO$_2$-HC(NH$_2$)$_2$PbI$_3$/ spiro-OMeTAD/Au	19.9	0.91	0.66	12.0	76

*bl-: blocking layer, mp-: mesoscopic porous

nanorods.[93] Devices employing FTO/glass substrate with with nanoparticles give a PCE of 5.5%. Flexible devices on PET/ITO with nanorods exhibit a PCE of 2.6%, while with nanoparticles yield a PCE of 2.2%. The devices on FTO substrate are generally better than devices on PET/ITO, because of the lower inherent resistance. Son *et al.* immersed ZnO seed layer in solution and grew ZnO nanorods.[98] The APCE of devices with ZnO is higher than that of devices with TiO$_2$ counterpart, while light harvesting efficiency is similar. This suggests the charge collection limits the current density in TiO$_2$ based PSC. The higher V_{OC} of devices based on ZnO is attributed to less recombination.

Some PSCs employ another layer between ZnO nanorod and perovskite. Usually, this layer modifies the interface to change the energy level or reduce recombination. Dong *et al.* introduced Al-doped ZnO (AZO) shell on ZnO nanoparticles.[99] The CBM of ZnO can be raised slightly using a small amount of Al to substitute the Zn site. AZO also gives higher electron mobility.[100] It is observed that the highest PCE of 10.5% occurs at 5% Al doping.[99] There is almost no change in J_{SC} when Al doping concentration in the AZO is less than 10%, but the J_{SC} decreases with higher concentration. Liu *et al.* deposited CdS quantum dots on ZnO nanorods to form ZnO/CdS-core/shell nanoarray acting as the electron-selective layer.[101] Though photoluminescence spectrum demonstrates that rich amount of defects on ZnO nanorod, they are effectively passivated by the CdS shell. The authors speculate that the increase in V_{OC} is due to the increased quasi-Fermi level in ZnO.

There are variations based on ZnO nanorods. He *et al.* grew aligned ZnO nano-obelisks on stainless steel wire to form solar cell fibers and fabrics.[102] The coaxial structure of the solar cell fibre makes the PCE insusceptible to the angle of incidence.

nanorods give a PCE of 8.9%, while those using FTO/glass The PSC maintains 93% of its initial efficiency after bending for 200 cycles, showing high stability. Mahmood *et al.* devised a double layer with ZnO nanorods on ZnO nanosheets.[85] They achieved a PCE of 10.35% and high stability. The efficiency remains more than 80% of the initial value after 240 hours, and J_{SC} is nearly constant. PSCs employing ZnO as ETM have been summarized in Table 3.

4. Other materials used in mesoscopic solar cell

Insulators, such as Al$_2$O$_3$, ZrO$_2$ and SiO$_2$, are used in PSC to take the place of mesoporous TiO$_2$. Among these materials, Al$_2$O$_3$ is the earliest and most widely adopted one, and devices of high efficiency have been obtained.[37] Different from TiO$_2$ and ZnO, Al$_2$O$_3$ is an insulator with wide band gap (7-9 eV) and Al$_2$O$_3$ nanoparticles purely act as a scaffold. Thus, for Al$_2$O$_3$-based cells, the electrons must be transported through the film thickness in the perovskite until they are collected at the planar TiO$_2$-coated FTO electrode. But chemical capacitance, caused by a high density of sub-band gap states, can be excluded by the insulating nature of Al$_2$O$_3$, leading to higher V_{OC}.[9] And the stability of devices with alumina scaffold is much better because there is no electron trapping in these devices, but there are traps in aged TiO$_2$-based solar cells arising from light-induced desorption of surface-absorbed oxygen, especially after being illuminated by ultraviolet light for a long time.[103] A post-modification by aluminium oxide, immersing the substrates coated with perovskite into triethylaluminum hexane solution, can protect perovskite and sensitized film from degradation by moisture and sunlight, and

Table 3 Summary of different PSCs with ZnO as ETM

ZnO morphology	Device structure	J_{SC} (mA/cm^2)	V_{OC} (V)	FF	PCE(%)	Ref
Compact layer	ITO/ ZnO/ MAPbI$_3$/ spiro-OMeTAD/ Ag	19.9	1.07	0.65	13.9	92
Compact layer	ITO/ ZnO/ C3-SAM/ MAPbI$_3$/spiro-OMeTAD/ MoO$_3$/ Ag	22.5	1.07	0.65	15.7	81
Compact layer	FTO/ ZnO/ MAPbI$_3$/ C	20.0	0.81	0.54	8.7	87
Compact layer	PEN/ ITO/ ZnO/ MAPbI$_3$/ C	13.4	0.76	0.42	4.3	87
Compact layer	PET/ ITO/ ZnO/ MAPbI$_3$/ spiro-OMeTAD/ Ag	13.4	1.03	0.74	10.2	88
Compact layer	ITO/ ZnO/ MAPbI$_3$/spiro-OMeTAD/Ag	20.4	1.03	0.75	15.7	88
Compact layer	FTO/ ZnO/ mp-Al$_2$O$_3$-MAPbI$_3$/spiro-OMeTAD/ Ag	20.4	0.98	0.66	13.1	86
Compact layer	FTO/ bl- ZnO/ CH$_3$NH$_3$PbI$_3$/ spiro-OMeTAD/Au	11.3	1.08	0.45	5.5	93
Compact layer	PET/ ITO/ bl-ZnO/ MAPbI$_3$/ spiro-OMeTAD/ Au	5.6	0.99	0.40	2.2	93
Compact layer	ITO/ ZnO / MAPbI$_3$/ spiro-OMeTAD/ Ag	23.1	0.89	0.50	10.3	94
Compact layer	FTO/ ZnO/ MAPbI$_3$/ spiro-OMeTAD/ Ag	16.0	1.01	0.67	10.8	95
Compact layer	FTO/ AZO/ MAPbI$_3$/ spiro-OMeTAD/ Ag	15.1	1.05	0.76	12.0	95
Compact layer	ITO/ ZnO/ PCBM/ MAPbI$_3$/PTB7-Th/ MnO$_x$/ Ag	14.7	1.02	0.73	11.0	82
Compact layer	ITO/ ZnO/ MAPbI$_3$/spiro-OMeTAD/ MnO$_x$/ Ag	18.2	1.00	0.67	12.2	82
Compact layer + nanorod	FTO/ bl-ZnO/mp-ZnO-MAPbI$_3$/spiro-OMeTAD/ Au	17.0	1.02	0.51	8.9	93
Compact layer + nanorod	PET/ ITO/ bl-ZnO/ mp-ZnO-MAPbI$_3$/ spiro-OMeTAD/ Au	7.5	0.80	0.43	2.6	93
nanorod	ITO/ ZnO/ MAPbI$_3$/ spiro-OMeTAD/ MoO$_3$/ Ag	22.4	1.04	0.57	13.4	89
nanorod	FTO/ bl- ZnO/mp-ZnO/ AZO shell/ MAPbI$_3$/spiro-OMeTAD/ Au	19.8	0.90	0.60	10.7	99
nanorod	FTO/ bl- ZnO/mp-ZnO-MAPbI$_3$/spiro-OMeTAD/ Au	20.1	0.99	0.56	11.1	98

*bl-: blocking layer, mp-: mesoscopic porous

retard the electron recombination at the perovskite/HTL interface.[104] Besides, Al$_2$O$_3$ scaffold also plays an important role in low-temperature fabricating PSC,[37,39,105] because the sinter process (~500 ^{o}C) is not necessary for Al$_2$O$_3$. And spin-coating an alumina/perovskite co-deposition suspension can simplify the fabricating process, making more convenience for mass production.[106]

ZrO$_2$ and SiO$_2$, as insulators as well, are similar to Al$_2$O$_3$. ZrO$_2$ is used both in devices with typical mesoscopic structure[107] and an efficient carbon-electrode device,[108] showing the potential of ZrO$_2$ nanoparticles in economical solar cells. The infiltration of perovskite is more important for such insulating mesoporous layers, so the pore size should be well concerned. SiO$_2$ nanoparticles with various diameters were synthesized via sol-gel method. It's found that the infiltration is optimized by controlling the size of the particle to 50 nm.[109] This result may be useful to the design of device with a mesoporous insulator layer. Snaith et al.[110] added Au@SiO$_2$ core-shell nanoparticles, synthesized with the assistance of PVP, to the Al$_2$O$_3$ colloid solution prior to the porous alumina film deposition. The presence of gold core possibly reduced the exciton binding energy and hence enhanced generation of free charge carriers, leading to an improved J_{SC}.

Some hole conductors can also be used to modify the interface and suppress charge recombination. For example, NiO is a p-type semiconductor with CBM at -1.8 eV and VBM at -5.2 eV.[111] Liu et al. fabricated perovskite solar cells with NiO as an interfacial layer, and found that the hole transfer and electron blocking ability of NiO results in faster charge transfer and less recombination compared to those with ZrO$_2$.[111] The 11.4% efficiency is 39% higher than those with ZrO$_2$.

Other semiconductors, SrTiO$_3$ (STO), WO$_3$ and SnO$_2$, are employed to take the place of TiO$_2$. STO has a wide band gap similar to that of TiO$_2$, but its CBM is slightly higher, matching better with the band structure of perovskite, which is beneficial

for electron collection. And the room-temperature electron mobility of bulk STO is much higher than that of TiO$_2$. In addition, the ferroelectricity of STO helps to reduce charge recombination at the interface. Therefore, devices based on mesoporous STO layer exhibits ~25% higher V_{OC} than that of conventional ones, however, accompanied by a decrease in photocurrent due to the large size of STO particles, which requires further improvement.[112] The band gap of WO$_3$ is comparatively smaller than TiO$_2$, but it has been shown to have higher carrier mobility than TiO$_2$. Furthermore, WO$_3$ can be synthesized into a wide range of nanostructures by electrospraying method.[113,114] Devices with ETL consisting of various WO$_3$ nanostructures were fabricated, and the device performance with WO$_3$ nanosheets is the best. In addition, a thin layer applied to the surface of WO$_3$ nanostructures can suppress charge recombination at the WO$_3$/perovskite interface, enhancing much higher V_{OC} and PCE.[115] SnO$_2$ has excellent electronic and optical properties, such as good antireflection, suitable band edge position and high charge mobility, and thus was used as ETL in PSC recently.[116,117] Ma et al.[116] reported a SnO$_2$ compact layer prepared by sol-gel method. Device based on such layer showed a surprisingly high J_{SC} of 30.99 mA/cm^2 due to high electron mobility but comparatively lower V_{OC} and FF than traditional PSC, which resulted from serious recombination at the interface. But this disadvantage may be corresponded to the quality of the layer and didn't appear in another work. Yan et al.[117] fabricated the SnO$_2$ compact layer by spin coating SnCl$_2$ · H$_2$O precursor and followed by annealing in air enhancement of J_{SC} and no reduction of V_{OC} and FF are observed, contributing to a PCE as high as 17.2%. These works demonstrate that SnO$_2$ is a promising ETM and has the potential to take the leading place of TiO$_2$. The performance of devices using these materials is compared in Table 4.

Table 4 Summary of different PSCs using other materials

Material	Device structure	J_{SC} (mA/cm^2)	V_{OC} (V)	FF	PCE(%)	Ref
Al$_2$O$_3$	FTO/ bl-TiO$_2$/mp-Al$_2$O$_3$-MAPbI$_{3-x}$Cl$_x$/spiro-OMeTAD/ Ag	18.0	1.02	0.67	12.3	105
Al$_2$O$_3$	FTO/graphene-TiO$_2$/mp-Al$_2$O$_3$-MAPbI$_3$/spiro-OMeTAD/Au	21.9	1.04	0.73	15.6	37
ZrO$_2$	FTO/ bl-TiO$_2$/mp-ZrO$_2$-MAPbI$_3$/spiro-OMeTAD/ Ag	17.3	1.07	0.59	10.8	107
TiO$_2$+ZrO$_2$	FTO/bl-TiO$_2$/mp-TiO$_2$-ZrO$_2$-(5-AVA)$_x$(MA)$_{1-x}$PbI$_3$/ C	22.8	0.86	0.66	12.8	108
SiO$_2$	FTO/ bl-TiO$_2$/mp-SiO$_2$-MAPbI$_3$/spiro-OMeTAD/ Au	16.4	1.05	0.66	11.5	109
Al$_2$O$_3$+Au@SiO$_2$	FTO/ bl-TiO$_2$/mp-Al$_2$O$_3$ -Au@SiO$_2$-MAPbI$_3$/spiro-OMeTAD/ Ag	16.9	1.02	0.64	11.4	110
SrTiO$_3$	FTO/ bl-TiO$_2$/mp-SrTiO$_3$-MAPbI$_{3-x}$Cl$_x$/spiro-OMeTAD/ Au	16.8	0.81	0.53	7.2	112
WO$_3$ + TiO$_2$	FTO/ bl-WO$_3$/mp-WO$_3$-MAPbI$_3$/spiro-OMeTAD/ Ag	17.0	0.87	0.76	11.2	115
SnO$_2$	FTO/ bl-SnO$_2$/ MAPbI$_3$/spiro-OMeTAD/ Au	23.3	1.11	0.67	17.2	117

*bl-: blocking layer, mp-: mesoscopic porous

5. Conclusion and outlook

In this review, we have given an overview of nanostructured electron transporting material for perovskite solar cells. Two main aspects of the ETL should be focused: material and morphology. In terms of material, TiO$_2$ is the most widely used ETM, and the synthesis and modification method of TiO$_2$ have matured and been mastered by most researchers. More importantly, devices employing TiO$_2$ as the ETM exhibit the highest PCE, which demonstrates that TiO$_2$ is still the most appropriate ETM for PSC until now. Traditional TiO$_2$ fabricating technique needs sintering process and defects in TiO$_2$ crystal grains aggravate the stability of devices, obstructing the large-scale application of TiO$_2$-based PSC. Sintering process can be avoided by using low-temperature fabricating methods, and conducting various modifications, such as different synthesis methods and doping, will improve the electronic property and stability. ZnO has much higher electron mobility than TiO$_2$, and thus gives better conductivity. ZnO doesn't require sintering process, ensuring that it can be used in flexible PSC, which is convenient to mass production. But similar to TiO$_2$, ZnO also suffers from photocorrosion, leading to unsatisfying stability. The PCE of ZnO-based devices is relatively lower than TiO$_2$-based ones. Further improvement for ZnO ETL is needed. Transparent insulators, Al$_2$O$_3$, ZrO$_2$ and SiO$_2$, purely serve as scaffold of perovskite. They can enhance stability and V_{OC} significantly, however, at the expense of conductivity. More and more new ETMs, such as SrTiO$_3$, WO$_3$ and SnO$_2$, have been applied in PSC. Remarkably, SnO$_2$ is very similar to TiO$_2$ but its electron mobility is much higher, leading to surprisingly high J_{SC}, which makes SnO$_2$ a promising material in PSC. In addition, the properties of ETL can be improved by incorporating some functional structures as well. Plasmonic Au-Ag alloy popcorn-shaped nanoparticles are employed in mesoporous TiO$_2$ layer, resulting in broader optical absorption and faster charge transfer.[118]

The morphology of ETL affects its performance as well. A thin compact layer with few pores and defects, acting as selective layer, is needed in most PSCs. The morphology of this compact layer can be controlled by different synthesis methods, such as solution synthesis, ALD, and magnetron sputtering. Mesoporous layer containing thousands of nanostructures can give the device better charge collection. Nanoparticles with rough surface provide large contact area between ETL and perovskite, but recombination is serious at the interface. This problem can be solved by coating the surface of nanoparticles with other material. Nanorod array has an open structure and a higher electron mobility suppressing the recombination, but nanorods aren't overall superior to nanoparticles due to the loss of rough surface. Some other nanostructures, such as 1D-nanowire, 3D-nanowire, nanotube, nanofiber, nanocone and nanohalice are synthesized and tested in PSC. Each of these nanostructures exhibits unique optical and electronic properties.

Precise control of components, geometrical factors and morphology of ETL may be an efficient method to further improve the performance of devices. But it requires a deeper understanding of the electron transporting mechanism in PSC, especially at the perovskite/ETL interface.

Acknowledgements

Notes and references

[a]State Key Laboratory for Mesoscopic Physics and Department of Physics, Peking University, [b]Beijing Engineering Research Center for Active Matrix Display, Beijing 100871, China

ᶜNew Display Device and System Integration Collaborative Innovation Center of the West Coast of the Taiwan Strait, Fuzhou 350002, China

1   D. B. Mitzi, *J. Mater. Chem.*, 2004, **14**, 2355–2365.
2   D. B. Mitzi, C. A. Feild, W. T. A. Harrison and A. M. Guloy, *Nature*, 1994, **369**, 467–469.
3   D. B. Mitzi, J. Chem. Soc., *Dalton Trans.*, 2001, 1–12.
4   T. Baikie, Y. Fang, J. M. Kadro, M. Schreyer, F. Wei, S. G. Mhaisalkar, M. Grätzel and T. J. White, *J. Mater. Chem. A*, 2013, **1**, 5628–5641.
5   S. A. Bretscheider, J. Weickert, J. A. Dorman and L. Schmidt-Mende, *APL Mater.*, 2014, **2**, 040701.
6   S. Colella, E. Mosconi, P. Fedeli, A. Listorti, F. Gazza, F. Orlandi, P. Ferro, T. Besagni, A. Rizzo, G. Calestani, G. Gigli, F. D. Angelis and R. Mosca, *Chem. Mater.*, 2013, **25**, 4613–4618.
7   A. Kojima, K. Teshima, Y. Shirai and T. Miyasaka, *J. Am. Chem. Soc.*, 2009, **131**, 6050–6051.
8   H.-S. Kim, C. R. Lee, J. H. Im, K. B. Lee, T. Moehl, A. Marchioro, S. J. Moon, R. Humphry-Baker, J. H. Yum, J. E. Moser, M. Grätzel and N. G. Park, *Sci. Rep.*, 2012, **2**, 591.
9   M. M. Lee, J. Teuscher, T. Miyasaka, T. N. Murakami and H. J. Snaith, *Science*, 2012, **338**, 643–647.
10   J. Burschka, N. Pellet, S.-J. Moon, R. Humphry-Baker, P. Gao, M. K. Nazeeruddin and M. Grätzel, *Nature*, 2013, **499**, 316–319.
11   H. Zhou, Q. Chen, G. Li, S. Luo, T. Song, H.-S. Duan, Z. Hong, J. You, Y. Liu and Y. Yang, *Science*, 2014, **345**, 542-546.
12   W. S. Yang, J. H. Noh, N. J. Jeon, Y. C. Kim, S. Ryu, J. Seo, S. I. Seok, *Science*, 2015, **348**, 1234-1237
13   http:// www. nrel.gov/
14   E. Edri, S. Kirmayer, A. Henning, S. Mukhopadhyay, K. Gartsman, Y. Rosenwaks, G. Hodes and D. Cahen, *Nano. Lett*, 2014, **14**, 1000-1004
15   G. Xing , N. Mathews , S. Sun , S. S. Lim , Y. M. Lam , M. Grätzel, S. Mhaislkar , T. C. Sum , *Science*, 2013, **342**, 344-347 .
16   S. D. Stranks , G. E. Eperon , G. Grancini , C. Menelaou ,M. J. P. Alcocer , T. Leijtens , L. M. Herz , A. Petrozza , H. J. Snaith, *Science*, 2013 , **342** , 341-344
17   H.-S. Kim , I. Mora-Sero , V. Gonzalez-Pedro , F. Fabregat-Santiago ,E. J. Juarez-Perez , N.-G. Park , J. Bisquert , *Nat. Commun*, 2013 , **4** ,2242 .
18   W. J. Potscavage, A. Sharma and B. Kippelen, *Accounts of Chemical Research*, 2009, **42**, 1758-1767.
19   H. S. Jung and N. -G. Park, *Small*, 2015, **11**, 10-25.
20   H. Tang, F.Levy, H.Berger and P.E.Schimid, *Phys. Rev. B*, 1995,**52**,7771
21   F. Arntz and Y. Yacoby, *Phys. Re*V. *Lett.* 1966, **17**, 857-859.
22   C. S. Ponseca Jr. , T. J. Savenije , M. Abdellah , K. Zheng , A. Yartsev ,T. Pascher , T. Harlang , P. Chabera and V. Sundstrom, *J. Am. Chem. Soc.*, 2014 , **136**, 5189-5192.
23   A. Hayakawa, O. Yoshikawa, T. Fujieda, K.Uehara and S. Yoshikawa, *Appl. Phys. Lett.*, 2007, **90**, 163517.
24   L. Kavan and M. Grätzel, *Electrochmica Acta*, 1995, **40**, 643-652.
25   P. Cameron and L. Peter, *J. Phys. Chem. B*, 2003, **107**, 14394-14400.
26   S.Ito, P. Liska, P. Comte, R. Charvet, P. Pechy, U. Bach, L. Schimidt-Mende, S. Zakeeruddin, A. Kay, M. Nazeeruddin, *Chem. Commun.*, 2005, **34**, 4351-4353.
27   J.N. Hart, D. Menzies, Y. Cheng, G.P. Simon, L. Spiccia, *C. R. Chimie*, 2006, **9**, 622-629.
28   T. Moehl, J. H. Im, Y. H. Lee, K. Domanski, F. Giordano, S. M. Zakeeruddin, M. I. Dar, L. -P. Heiniger, M. K. Nazeeruddin, N. Park and M. Grätzel, *J. Phys. Chem. Lett.*, 2014, **5**, 3931-3936.
29   Y. Wu, X. Yang, H. Chen, K. Zhang, C. Qin, J. Liu, W. Peng, A.Islam, E. Bi, F. Ye, M. Yin, P. Zhang and L. Han, *Appl. Phys. Express*, 2014, **7**, 052301.
30   W. Ke, G. J. Fang, J. Wang, P. L. Qin, H. Tao, H. W. Lei, Q. Liu, X. Dai and X. Z. Zhao, *ACS Appl. Mater. Inter.,* 2014, **6**, 15959.
31   Q. Gao, S. Yang, L. Lei, S. Zhang, Q. Cao, J. Xie, J. Li and Y. Liu, *Chem. Lett.*, 2015, **44**, 624-626.
32   J. Wang, M. Qin, H. Tao, W. Ke, Z. Chen, J. Wan, P. Qin, L. Xiong, H. Lei, H. Yu and G. Fan, *Appl. Phys. Lett.*, 2015, **106**, 121104.
33   A. K. Ghosh , F. G. Wakim , R. R. Addiss , *Phys. Rev.* 1969 , **184** , 979-&.
34   S. Wendt, P. T. Sprunger, E. Lira, G. K. H. Madsen, Z. Li, J. Ø. Hansen, J. Matthiesen, A. Blekinge-Rasmussen, E. Laegsgaard, B. Hammer and F. Besenbacher , *Science,* 2008 , **320** , 1755-1759.
35   S.K. Pathak, K. Sandeep, A. Abate, P. Ruckdeschel, H. J. Snaith and U. Steiner, *Adv. Funct. Mater.*, 2015, **24**, 6046-6055.
36   X. Yin, Y. Guo, Z. Xue, P. Xu, M. He and B. Liu, *Nano. Res.* 2015, DOI 10.1007/s12274-015-0711-4
37   J. T. W. Wang, J. M. Ball, E. M. Barea, A. Abate, J. A. Alexander-Webber, J. Huang, M. Saliba, I. N. Mora-Sero, J. Bisquert, and H. J. Snaith, *Nano Lett*. 2014, **14**, 724-730.
38   A. Yella, L. Heiniger, P. Gao, M. K. Nazeeruddin and M. Grätzel, *Nano lett*, 2014, **14**, 2591-2596.
39   K. Wojciechowski, M. Saliba, T. Leijtens, A. Abate and H.J. Snaith, *Energy. Environ. Sci*, 2014,**7**, 1142-1147.
40   M. M. Lee, J. Teuscher, T. Miyasaka, T. N. Murakami, J. Henry, *Science*, 2012, **338**, 643–647.
41   B. Conings, L. Baeten, T. Jacobs, R. Dera, J. D'Haen, J. Manca and H. -G. Boyen, *APL Mater.* 2014, **2**, 081505.
42   L. Zheng, D. Zhang, Y. Ma, Z. Lu, Z. Chen, S. Wang, L. Xiao and Q. Gong, *Dalton Trans.*, 2015, **44**, 10582-10593.
43   J.-W. Lee , T.-Y. Lee , P. J. Yoo , M. Grätzel , S. Mhaisalkar and N.-G. Park, *J. Mater. Chem. A*, 2014 , **2** , 9251-9259.
44   V. Gonzalez-Pedro , E. J. Juarez-Perez , W.-S. Arsyad , E. M. Barea ,F. Fabregat-Santiago , I. Mora-Sero and J. Bisquert, *Nano Lett.*, 2014, **14**, 883-893.
45   I. C. Baek, M. Vithal, J. A. Chang, J.-H. Yum, M. K. Nazeeruddin, M. Grätzel, Y.-C. Chung,and   S. I. Seok, *Electrochem. Commun*. 2009, **11**, 909-912..
46   J. A. Chang, J. H. Rhee, S. H. Im, Y. H. Lee, H. Kim, S. I Seok,. Md. K. Nazeeruddin, and M. Grätzel, *Nano Lett.* 2010,**10**, 2609–2612.
47   J. H. Noh, S. H. Im, J. H. Heo, T. N. Mandal and S. I. Seok, *Nano Lett*. 2013, **13**, 1764-1769.
48   N. R. Neale and A. J. Frank, *J. Mater. Chem*. 2007, **17**, 3216.
49   Y. Yang, K.Ri, A. Mei, L. Liu, M. Hu, T. Liu, X. Li and H. Han, *J. Mater. Chem. A*, 2015, **3**, 9103-9107.
50   A. Sarkar, N. J. Jeon, J. H. Noh and S I. Seok, *J. Phys Chem. C*, 2014, **118**, 16688-16693.
51   E. J. W. Crossland, N. Noel, V. Sivaram, T. Leijtens, J. A. Alexander-Webber and H. J. Snaith, *Nature*, 2013, **495**, 215-219.
52   A. K. Chandiran, A. Yella, M. T. Mayer, P. Gao, M. K. Nazeeruddin and M. Grätzel, *Adv. Mater.* 2014, **26**, 4309-4312.
53   G. S. Han, H. S. Chung, B. J. Kim D. H. Kim, J. W. Lee, B. S. Swain, K. M. Mahmood, J. S. Yoo, N. -G. Park, J. H. Lee and H. S. Jung, *J. Mater. Chem. A*. 2015, **3**, 9160-9164.
54   P. Qin, A. L. Domanski, A. K. Chandiran, R. Berger, H. -J. Butt, M. I. Dar, T. Moehl, N. Tetreault, P. Gao, S. Ahmad, M. K. Nazeeruddin and M. Grätzel, *Nanoscale*, 2014, **6**, 1508-1514.
55   A. Abrusci, S. D. Stanks, P. Docampo, H. -L. Yip, A. K.-Y Jen and H. J. Snaith, *Nano. Lett*., 2013, **13**, 3124-3128.
56   Z. Zhu, J. Ma, Z. Wang, C. Mu, Z. Fan, L. Du. Y, Bai, L. Fan, H. Yan, D. L. Philips and S. Yang, *J. Am. Chen. Soc*, 2014, **136**, 3760-3763.
57   M. Zhang, L. Bai, W. Shang, W. Xie, H, Ma, Y, Fu, D. Fang, H. Sun, L. Fan, M. Han, C. Liu and S. H. Yang, *J. Mater. Chem.*, 2012, **22**, 7461-7467.

Nanoscale Accepted Manuscript

58 H.-S. Kim, J.-W. Lee, N. Yantara, P. P. Boix, S. A. Kulkarni, S. Mhaisalkar, M. Grätzel and N.-G. Park, *Nano Lett*. 2013, **13**, 2412–2417.

59 J.-J. Wu and C.-C. Yu, *J. Phys. Chem. B*, 2004, **108**, 3377-3379..

60 K. Zhu, N. R. Neale, A. Miedaner and A. J. Frank, *Nano Lett.*, 2007, **7**, 69-74.

61 B. Liu and E. S. Aydil, *J. Am. Chem. Soc.,* 2009, **131**, 3985-3990.

62 B. Cai, D. Zhong, Z. Yang, B. Huang, S. Miao, W. -H. Zhang, J. Qiu and C. Li, *J. Mater. Chem. C*, 2015, **3**, 729-733.

63 A. Fakharuddin, F. D. Giacomo, I. Ahmed, Q. Wali, T. M. Brown and R. Jose, *J. Pow. Sour*, 2015, **283**, 61-67.

64 S. S. Mali, C. S. Shim, H. K. Park, J. Heo, P. S. Patil and C. K. Hong, *Chem. Mater*, 2015, **27**, 1541-1551.

65 K. Manseki, T. Ikeya, A. Tamura, T. Ban, T. Sugiura and T. Yoshida, *RSC. Adv*, 2014, **4**, 9652-9655.

66 M. Yang, R. Guo, K. Kadel, Y. Liu, K. O'shea, R. Bone, X. Wang, J. He and W. Li, *J. Mater. Chem. A*,2014, **2**, 19616-19622.

67 X. Zhang, Z. Bao, X. Tao, H. Sun, W. Chen and X. Zhou, *RSC. Adv*, 2014, **4**, 64001-64005.

68 Y. Liao , W. Que, Q. Jia, Y. He, J. Zhang and P. Zhong, *J. Mater. Chem*, 2012, **22**, 7937-7944.

69 J. Qiu, Y. Qiu, K. Yan, M. Zhong, C. Mu, H. Yan and S. Yang, *Nanoscale*, 2013, **5**, 3245-3248.

70 Q. Jiang, X. Sheng, Y. Li, X. Feng and T. Xu, *Chem. Commun*, 2014, **50**, 14720-14723.

71 Y. Yu, J. Li, D. Geng, J. Wang, L. Zhang, T. L. Andrew, M. S. Arnold and X. Wang, *ACS. Nano*,2015, **9**, 564-572.

72 X. Gao, J. Li, J. Baker, Y. Hou, D. Guan, J. Chen and C. Yuan, *Chem. Commun*, 2014, **50**, 6368-6371.

73 X. Wang, Z. Li, W. Xu, S. A. Kulkarni, S. K. Batabyal, S. Zhang, A. Cao and L. H. Wong, *Nano. Energy*, 2015, **11**, 728-735.

74 S. Dharani, H. K. Mulmudi, N. Yantara, P. T. T.Trang, N. G. Park, M. Grätzel, S. Mhaisalkar, N. Mathews and P. P. Boix, *Nanoscale*, 2014, **6**, 1675-1679.

75 D. Zhong, B. Cai, X. Wang, Z. Yang, Y. Xing, S. Miao, W.-H. Zhang and C. Li, *Nano. Energy*, 2015, **11**, 409-418.

76 J. -W. Lee, S. H. Lee, H. -Seok Ko, J. Kwon, J. H. Park, S. M. Kang, N. Ahn, M. Choi, J. K. Kim and N. -G. Park, *J. Mater. Chem. A.*, 2015, **3**, 9179-9186.

77 S. Hwang, H. Kwon, S. Chhajed, J. W. Byon, J. M. Baik, J. Im,, S. H. Oh, H. W. Jang, S. J. Yoon and J. K. Kim, *Analyst*, 2013, **138**, 443–450.

78 Y.-P. Zhao, D.-X. Ye, G.-C. Wang and T.-M. Lu, *Proc. SPIE*, 2003, **5219**, 59–73.

79 H. Kwon, J. Ham, D. Y. Kim, S. J. Oh, S. Lee, S. H. Oh, E. F. Schubert, K.-G. Lim, T.-W. Lee, S. Kim, J.-L. Lee and J. K. Kim, *Adv. Energy Mater*. 2014, **4**, 1301566.

80 C. Xu, X. Sun, Z. Dong, G. Zhu and Y. Cui, *Appl.Phys. Lett.*, 2006, **88**, 093101.

81 L. Zuo, Z. Gu, T. Ye, W. Fu, G. Wu, H. Li and H. Chen, *J. Am. Chem. Soc.*, 2015, **137**, 2674-2679.

82 J. Kim, G. Kim, T. K. Kim, S. Kwon, H. Back, J. Lee, S. H. Lee, H. Kang and K. Lee, *J. Mater. Chem. A.*, 2014, **2**, 17291-17296.

83 C. Magne, T. Moehl, M. Urien, M. Gratzel and T. Pauporte, *J. Mater. Chem. A.*, 2013, **1**, 2079-2088.

84 M. Law, L. E. Greene, J. C. Johnson, R. Saykally and P. D. Yang, *Nat. Mater.*, 2005, **4**, 455-459.

85 K. Mahmood, S. S. B and A. Amassian, *Nanoscale*, 2014, **6**, 14674-14678.

86 X. Dong, H. Hu, B. Lin, J. Ding and N. Yuan, *Chem. commun.*, 2014, **50**, 14405-14408.

87 H. Zhou, Y. Shi, K. Wang, Q. Dong, X. Bai, Y. Xing, Y. Du and T. Ma, *J. Phys. Chem. C.*, 2015, **119**, 4600-4605.

88 D. Liu and T. L. Kelly, *Nat. Photonics*, 2013, **8**, 133-138.

89 L. Liang, Z. Huang, L. Cai, W. Chen, B. Wang, K. Chen, H. Bai, Q. Tian and B. Fan, *ACS Appl. Mater. Inter.*, 2014, **6**, 20585-20589.

90 P. E. de Jongh, E. A. Meulenkamp, D. Vanmaekelbergh and J. J. Kelly, *J. Phys. Chem. B.,* 2000, **104***,* 7686-7693

91 H. Zhang, R. Zong, and Y. Zhu *J. Phys. Chem. C,* 2009, **113**, 4605–4611

92 J. Song, J. Bian, E. Zheng, X.-F. Wang, W. Tian and T. Miyasaka, *Chem. Lett.,* 2015, **44**, 610-612.

93 M. H. Kumar, N. Yantara, S. Dharani, M. Graetzel, S. Mhaisalkar, P. P. Boix and N. Mathews, *Chem. commun.*, 2013, **49**, 11089-11091.

94 J. Zhang, E. J. Juárez-Pérez, I. Mora-Seró, B. Viana and T. Pauporté, *J. Mater. Chem. A.*, 2015, **3**, 4909-4915.

95 K. Mahmood, B. S. Swain and H. S. Jung, *Nanoscale*, 2014, **6**, 9127-9138.

96 H. Ting, L.Ni, S.. Ma, Y. Ma, L. Xiao and Z. Chen, *Acta Phys. Sin*, 2015, **64**, 038802

97 B. Suarez, V. Gonzalez-Pedro, T. S. Ripolles, R. S. Sanchez, L. Otero and I. Mora-Sero, *J. Phys. Chem. Lett.*, 2014, **5**, 1628-1635.

98 D.-Y. Son, J.-H. Im, H.-S. Kim and N.-G. Park, *J. Phys. Chem. C.*, 2014, **118**, 16567-16573.

99 J. Dong, Y. Zhao, J. Shi, H. Wei, J. Xiao, X. Xu, J. Luo, J. Xu, D. Li, Y. Luo and Q. Meng, *Chem. commun.*, 2014, **50**, 13381-13384.

100 J. P. Deng, M. Q. Wang, J. Liu, X. H. Song and Z. Yang, *J Colloid Interf Sci*, 2014, **418**, 277-282.

101 C. Liu, Z. Qiu, W. Meng, J. Chen, J. Qi, C. Dong and M. Wang, *Nano Energy*, 2015, **12**, 59-68.

102 S. He, L. Qiu, X. Fang, G. Guan, P. Chen, Z. Zhang and H. Peng, *J. Mater. Chem. A.*, 2015, **3**, 9406-9410.

103 T. Leijtens, G. E. Eperon, S. Pathak, A. Abate, M. M. Lee and H. J. Snaith, *Nature. Commun*, 2013, **4**, 2885.

104 G. Niu, W. Li, F. Meng, L. Wang, H. Dong and Y. Qiu, *J. Mater. Chem. A*, 2014, **2**, 705-710.

105 J. M. Ball, M. M. Lee, A. Hey and H. J. Snaith, *Energy Environ. Sci*, 2013, **6**, 1739-1743.

106 M. J. Carnie, C. Charbonneau, M. L. Davies, J. Troughton, T. M Watson, K. Wojciechowski, H. J. Snaith and D. A. Worsley, *Chem. Commun*, 2013, **49**, 7893-7895.

107 D. Bi, S. -J. Moon, L. Häggman, G. Bosschloo, L. Yang, E. M. J. Johansson, M. K. Nazeeruddin, M. Grätzel and A. Hagfeldt, *RSC Adv*, 2013, **3**, 18762-18766.

108 A. Mei , X. Li , L. Liu , Z. Ku , T. Liu , Y. Rong , M. Xu , M. Hu , J. Chen ,Y. Yang , M. Grätzel and H. Han, *Science*, 2014 ,**345** ,295-298.

109 S. H. Hwang, J. Roh, J. Lee, J. Ryu, J. Yun and J. Jang, *J. Mater, Chem. A*, 2014, **2**, 16429-16433.

110 W. Zhang, M. Saliba, S. D. Stranks, Y. Sun, X. Shi, U. Wiesner and H. J. Snaith, *Nano. Lett*, 2013, **13**, 4505-4510.

111 Z. Liu, M. Zhang, X. Xu, L. Bu, W. Zhang, W. Li, Z. Zhao, M. Wang, Y. Cheng, and H. He, *Dalton Trans.*, 2015, **44**, 3967

112 A. Bera, K. Wu, A. Sheikh, E. Alarousu, O. F. Mohammed and T. Wu, *J. Phys. Chem. C,* 2014, **118**, 28494-28501.

113 S. K. Deb, *Sol. Energy Mater. Sol. Cells*, 2008, **92**, 245–258.

114 .H. S. Shim, J. W. Kim, Y. E. Sung and W. B. Kim, *Sol. Energy. Mater. Sol. Cells*, 2009, **93**, 2062–2068.

115 K. Mahmood, B. S. Swain, A. R. Kirmani, A. Amassian, *J. Mater. Chem. A*, 2015, **3**, 9051-9057.

116 Q. Dong, Y. Shi. K. Wang, Y. Li, S. Wang, H. Zhang, Y. Xing, Y. Du, X. Bai and T. Ma, *J. Phys, Chem. C*, 2015, **119**, 10212-10217

117 W. Ke, G. Fang, Q. Liu, L. Xiong, P. Qin, H. Tao, J. Wang, H. Lei, B. Li, J. Wan, G. Yang and Y. Yan, *J. Am. Chem. Soc*, 2015, **137**, 6730-6733

118 Z. Lu, X. Pan, Y. Ma, Y. Li, L. Zheng, D. Zhang, Q. Xu, Z. Chen, S. Wang, B. Qu, F. Liu, Y. Huang, L. Xiao and Q. Gong, *RSC Adv*, 2015, **5**, 11175-11179.